

FIG. 1: (Color online) A sketch of the junction.

is formed by D two-level systems with the levels representing ground (g) and excited (x) states of the molecule. Each of the two level systems is subjected to a classical local EM field $\vec{E}(t)$ (see section III for details of its calculation). Electron transfer is allowed along the chain of ground (excited) levels of the bridge. The contacts are taken in the form of bowtie antennas, and are assumed to be reservoirs of free electrons each in its own equilibrium with electrochemical potentials μ_L and μ_R , respectively (see Fig. 1). The Hamiltonian of the system reads (here and below $e = \hbar = 1$)

$$\hat{H}(t) = \hat{H}_M(t) + \sum_{K=L,R} (\hat{H}_K + \hat{V}_K) \quad (1)$$

$$\hat{H}_M(t) = \sum_{s=g,x} \left[\sum_{m=1}^D \varepsilon_s \hat{d}_{ms}^\dagger \hat{d}_{ms} - \sum_{m=1}^{D-1} t_s (\hat{d}_{m+1s}^\dagger \hat{d}_{ms} + H.c.) \right] - \sum_{m=1}^D (\vec{\mu}_{mg,mx} \hat{d}_{mg}^\dagger \hat{d}_{mx} + H.c.) \vec{E}_m(t) \quad (2)$$

$$\hat{H}_K = \sum_{k \in K} \varepsilon_k \hat{c}_k^\dagger \hat{c}_k \quad (3)$$

$$\hat{V}_K = \sum_{k \in K} \sum_{s=g,x} (V_{k,m_K s} \hat{c}_k^\dagger \hat{d}_{m_K s} + H.c.) \quad (4)$$

where $\hat{H}_M(t)$ and \hat{H}_K are Hamiltonians of the molecular bridge (M) and the contacts ($K = L, R$), and \hat{V}_K is coupling between them. In Eqs. (2)-(4) \hat{d}_{ms}^\dagger (\hat{d}_{ms}) and \hat{c}_k^\dagger (\hat{c}_k) are creation (annihilation) operators for an electron on the level s of the molecular bridge site m and state k of the contact, respectively. $\vec{E}_m(t)$ is the local time-dependent field at bridge site m , and $\vec{\mu}_{ms,ms'} = \langle ms | \hat{\vec{\mu}} | ms' \rangle$ is the matrix element of the transition molecular (vector) dipole operator between states $|ms\rangle$ and $|ms'\rangle$. For simplicity below we assume that the transition dipole moment is the same for all bridge sites and has only one non-zero component, $\mu_{mg,mx} \equiv \mu_{gx}$ for any m . t_s ($s = g, x$) and $V_{k,m_K s}$ are matrix elements for electron transfer in the molecular bridge and between molecule and contacts, respectively, and $m_K = 1$ (D) for $K = L$ (R). Note that treating the external field classically allows us to account for arbitrary time dependence exactly (i.e. beyond perturbation theory).⁴⁹

We follow the formulation of Ref. 49. Time-dependent

current at interface K (L or R) is⁶³

$$I_K(t) = -\text{Im Tr} \left[\mathbf{\Gamma}^K \left(\mathbf{G}^<(t, t) + \int \frac{d\epsilon}{\pi} f_K(\epsilon) \mathbf{G}^r(t, \epsilon) \right) \right] \quad (5)$$

where $\text{Tr}[\dots]$ is a trace over the molecular subspace, $f_K(\epsilon) \equiv [e^{(\epsilon - \mu_K)/T} + 1]^{-1}$ is the Fermi-Dirac distribution in contact K , $\mathbf{\Gamma}^K$ is the molecular dissipation matrix due to coupling to contact K

$$\mathbf{\Gamma}_{m_1 s_1, m_2 s_2}^K(\epsilon) \equiv 2\pi \sum_{k \in K} V_{m_1 s_1, k} V_{k, m_2 s_2} \delta(\epsilon - \varepsilon_k), \quad (6)$$

and $\mathbf{G}^<(r)$ is a matrix in the molecular basis of the lesser (retarded) projection of the single particle Green function, defined on the Keldysh contour as⁶⁴

$$G_{m_1 s_1, m_2 s_2}(\tau_1, \tau_2) \equiv -i \langle T_c \hat{d}_{m_1 s_1}(\tau_1) \hat{d}_{m_2 s_2}^\dagger(\tau_2) \rangle \quad (7)$$

Here T_c is the contour ordering operator and $\tau_{1,2}$ are the contour variables. In Eq.(5) $\mathbf{G}^r(t, \epsilon)$ is the right Fourier transform of the retarded projection of the Green function (7)

$$\mathbf{G}^r(t, \epsilon) \equiv \int dt' e^{i\epsilon(t-t')} \mathbf{G}^r(t, t') \quad (8)$$

Note that in Eq.(5) and below we assume the wide band limit⁶⁵ in the metallic contacts.

The Green functions in (5) satisfy the following set of equations of motions^{48,66}

$$i \frac{\partial}{\partial t} \mathbf{G}^r(t, \epsilon) = \mathbf{I} - \left(\epsilon \mathbf{I} - \mathbf{H}_M(t) + \frac{i}{2} \mathbf{\Gamma} \right) \mathbf{G}^r(t, \epsilon) \quad (9)$$

$$i \frac{d}{dt} \mathbf{G}^<(t, t) = [\mathbf{H}_M(t); \mathbf{G}^<(t, t)] - \frac{i}{2} \{ \mathbf{\Gamma}; \mathbf{G}^<(t, t) \} + i \sum_{K=L,R} \int \frac{d\epsilon}{2\pi} f_K(\epsilon) (\mathbf{\Gamma}^K \mathbf{G}^a(\epsilon, t) - \mathbf{G}^r(t, \epsilon) \mathbf{\Gamma}^K) \quad (10)$$

where \mathbf{I} is the unity matrix, $\mathbf{H}_M(t)$ is a representation of the operator (2) in the molecular basis, $\mathbf{\Gamma} \equiv \sum_{K=L,R} \mathbf{\Gamma}^K$, $[\dots; \dots]$ and $\{\dots; \dots\}$ are the commutator and anti-commutator, and $\mathbf{G}^a(\epsilon, t) \equiv [\mathbf{G}^r(t, \epsilon)]^\dagger$. The first order differential equations (9) and (10) are solved starting from the initial condition of the biased junction steady-state in the absence of the optical pulse, $E(t=0) = 0$

$$\mathbf{G}_0^r(\epsilon) \equiv \mathbf{G}^r(t=0, \epsilon) = \left[\epsilon \mathbf{I} - \mathbf{H}_M(t=0) + \frac{i}{2} \mathbf{\Gamma} \right]^{-1} \quad (11)$$

$$\mathbf{G}_0^< \equiv \mathbf{G}^<(t=0, t=0) = i \sum_{K=L,R} \int \frac{d\epsilon}{2\pi} \mathbf{G}_0^r(\epsilon) \mathbf{\Gamma}^K f_K(\epsilon) \mathbf{G}_0^a(\epsilon) \quad (12)$$

where $\mathbf{G}_0^a(\epsilon) \equiv [\mathbf{G}_0^r(\epsilon)]^\dagger$.

Below we calculate the charge pumped through the junction by the optical pulse

$$Q(t) \equiv \int_0^t dt' \frac{I_L(t') - I_R(t')}{2} - I_0 t \quad (13)$$

where $I_{L,R}(t)$ are defined in Eq.(5), and I_0 is the steady-state current

$$I_0 \equiv \int \frac{d\epsilon}{2\pi} \text{Tr} \left[\Gamma^L \mathbf{G}_0^r(\epsilon) \Gamma^R \mathbf{G}_0^a(\epsilon) \right] (f_L(\epsilon) - f_R(\epsilon)) \quad (14)$$

III. SELF-CONSISTENT ELECTRODYNAMICS

The time evolution of electric, \vec{E} , and magnetic, \vec{H} , fields is considered according to the set of Maxwell's equations (written here in SI units)

$$\mu_0 \frac{\partial \vec{H}(\vec{r}, t)}{\partial t} = -\vec{\nabla} \times \vec{E}(\vec{r}, t), \quad (15a)$$

$$\epsilon_0 \frac{\partial \vec{E}(\vec{r}, t)}{\partial t} = \vec{\nabla} \times \vec{H}(\vec{r}, t) - \vec{J}(\vec{r}, t), \quad (15b)$$

where μ_0 and ϵ_0 are the magnetic permeability and dielectric permittivity of the free space, respectively, and $\vec{J}(t)$ is the electric current density. Note that magnetization is disregarded in Eqs. (15a) and (15b), since we assume both molecule and contacts to be non-magnetic.

A molecule located at site m ($\equiv \vec{r}_m$) and driven by local electric field $\vec{E}(\vec{r}_m, t)$, yields time-dependent response, which enters Ampere's law as a polarization current density

$$\vec{J}(\vec{r}_m, t) = \frac{\partial \vec{P}_m(t)}{\partial t} \delta(\vec{r}_m), \quad (16)$$

where δ is the Dirac delta-function. The polarization depends on molecular characteristics through the molecular density matrix, which in turn is affected by the local field. In our model two-level systems of the molecular bridge (2) are assumed to occupy sites of the FDTD grid. Molecules contribute to the polarization at their site according to

$$\vec{P}_m(t) = 2 \text{Im} \left[\vec{\mu}_{mx,mg} G_{mg,mx}^<(t, t) \right] \quad (17)$$

The resulting system of coupled differential equations, Eqs (15)-(15b), is solved simultaneously with EOMs for the Green functions of the quantum system, Eqs. (9)-(10). The Maxwell's equations are discretized in time and space and propagated using the finite-difference time-domain approach (FDTD).⁶⁷ We employ three-dimensional FDTD calculations utilizing home-build parallel FORTRAN-MPI codes on a local multi-processor cluster.⁶⁸ In spatial regions occupied by a plasmonic nanostructure (a bowtie antenna in our case) we employ the auxiliary differential equation method to account for materials dispersion. The dielectric response of the metal is modeled using a standard Drude formulation with the set of parameters describing silver.^{48,49} The Green functions EOMs are propagated with the fourth order Runge-Kutta scheme.

Within described self-consistent model the local electric field $\vec{E}_m(t) \equiv \vec{E}(\vec{r}_m, t)$ in Eq.(2) driving a molecular

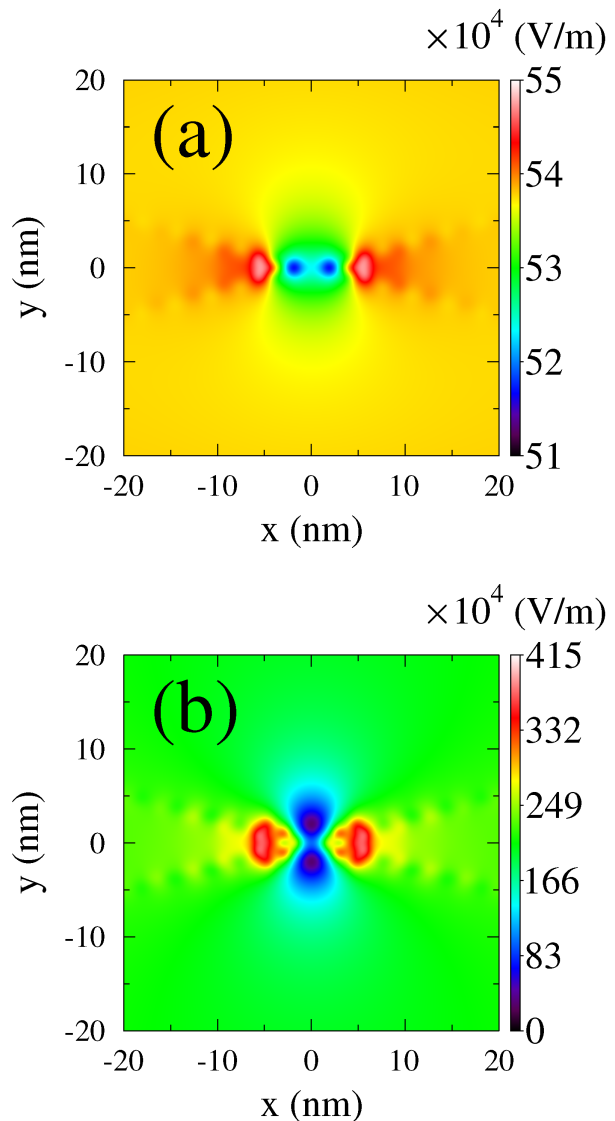


FIG. 2: (Color online) Map of the instantaneous electric field strength, $[E_x^2(\vec{r}, t) + E_y^2(\vec{r}, t) + E_z^2(\vec{r}, t)]^{1/2}$, at a distance of 10 nm from the molecule (the plane is parallel to xy) calculated (a) without and (b) with the molecular response. The distribution is shown for $t = 77.8$ fs and 81.7 fs for (a) and (b) respectively. See text for parameters.

junction is thus defined by both SPP excitations in the contacts and the local molecular response. In the next section we show that the molecular contribution changes junction transport characteristics drastically, and in general can not be ignored.

IV. NUMERICAL RESULTS

Here we present result of numerical simulations demonstrating the importance of a self-consistent treatment of the local EM field dynamics. Previous studies consid-

ered the influence of an isolated molecule on plasmon transfer,^{41,42,45} molecular features in absorption^{32,50,69,70} and Raman^{29,31,46} spectra of molecules attached to nanoparticles. Below we discuss how molecular junctions and electron transport are influenced by a local EM field and vice versa in a self-consistent manner.

Unless otherwise specified parameters of the calculations are $T = 300$ K, $\varepsilon_x = -\varepsilon_g = 1$ eV, $t_x = t_g = 0.05$ eV, $\mu_{gx} = 32$ D, $\Gamma_{1g,1g}^L = \Gamma_{Dx,Dx}^R = 0.1$ eV and $\Gamma_{1x,1x}^L = \Gamma_{Dg,Dg}^R = 0.01$ eV (other elements of the dissipation matrix are zero). These parameters are chosen to represent a molecular junction with a strong charge-transfer transition⁵⁹, and are similar to our previous considerations.^{48,49} The Fermi energy is taken at the origin, $E_F = 0$, and the bias is applied symmetrically, $\mu_L = -\mu_R = V_{sd}/2$.

Following Ref. 48, the incoming incident field is taken in the form of a chirped pulse

$$E_{\text{inc}}(t) = \text{Re} \left[\mathcal{E}_0 \exp \left(-\frac{(\delta^2 - i\bar{\mu}^2)t^2}{2} - i\omega_0 t \right) \right] \quad (18)$$

where \mathcal{E}_0 is the incident peak amplitude, ω_0 is the incident frequency, and $\delta^2 \equiv 2\tau_0^2/(\tau_0^4 + 4\Phi''^2(\omega_0))$ and $\bar{\mu} \equiv -4\Phi''(\omega_0)/(\tau_0^4 + 4\Phi''^2(\omega_0))$ are parameters describing the incident chirped pulse (τ_0 is the characteristic time related to the pulse duration). In the calculations below we use $\mathcal{E}_0 = 10^7$ V/m, $\omega_0 = 2$ eV, $\tau_0 = 11$ fs, and $\Phi''(\omega_0) = 3000$ fs².

Figure 2 shows instantaneous electric field strength distributions in a plane shifted by $z = 10$ nm parallel to xy plane. The distribution is calculated for a junction formed by bowtie antennas with single molecule ($D = 1$) placed in the center of the gap. Here $\varepsilon_x - \varepsilon_g = 1.75$ eV, $\Gamma_{1g,1g}^L = \Gamma_{Dx,Dx}^R = 0.01$ eV, $\Gamma_{1x,1x}^L = \Gamma_{Dg,Dg}^R = 0.001$ eV, and $V_{sd} = 0$. Fig. 2a presents simulations without molecular response. Fig. 2b shows results of a calculation where both SPP excitations in the contacts and molecular response are taken into account. One can clearly see that even a single molecule drastically changes local electric field distribution.

Sensitivity of the pulse temporal behavior to the molecular response is presented in Figure 3a. Here a local field affected by only SPP modes (dotted line) is compared to pulses calculated when molecular response is taken into account. The latter may result in both enhancement (dashed line) or quenching (solid line) of the local field depending on the ratio of the pulse frequency, ω_0 , to the molecular excitation energy, $\varepsilon_x - \varepsilon_g$. In particular, quenching is observed for the laser frequency being below the threshold ($\omega_0 < \varepsilon_x - \varepsilon_g = 2.25$ eV), while frequency above the threshold ($\omega_0 > \varepsilon_x - \varepsilon_g = 1.75$ eV) leads to enhancement of the field. To understand this behavior we perform a simple analysis treating coupling to the driving field as a perturbation, and neglecting the chirped

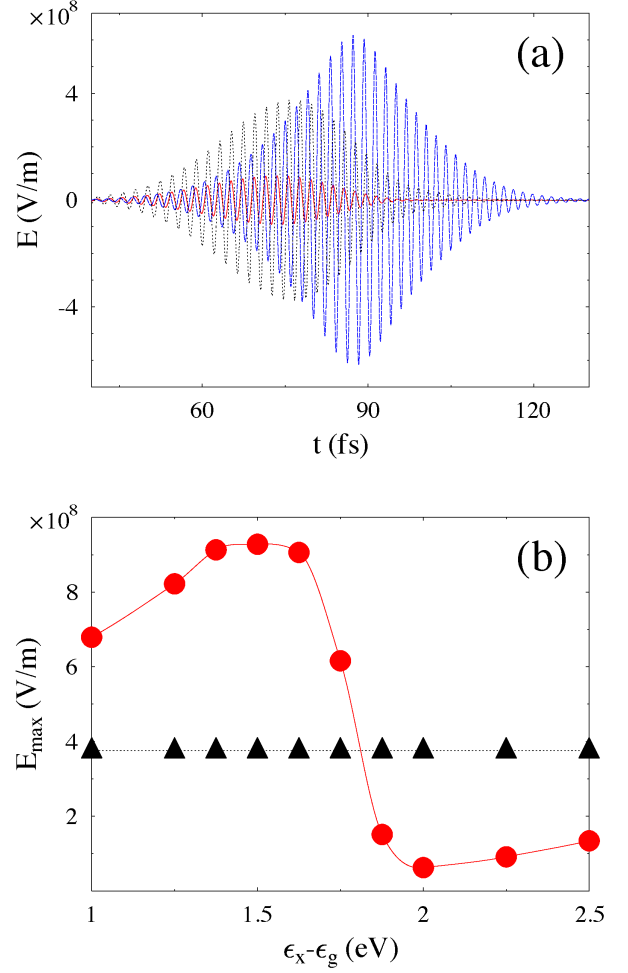


FIG. 3: (Color online) Local EM field at the molecular position. (a) Pulse calculated without (dotted line, black) and with ($\varepsilon_x - \varepsilon_g > \omega_0$ - solid line, red; $\varepsilon_x - \varepsilon_g < \omega_0$ - dashed line, blue) molecular response. (b) Maximum local field during the pulse vs. molecular excitation energy calculated without (triangles, black) and with (circles, red) molecular response. See text for parameters.

character of the pulse. This leads to (see Appendix A)

$$P_1(t) \approx -\mathcal{E}_0 \cos(\omega_0 t) |\mu_{gx}|^2 \int \frac{d\epsilon}{2\pi} \quad (19)$$

$$\left(\text{Im} [G_{1g,1g}^<(\epsilon)] \frac{\epsilon - (\varepsilon_x - \omega_0)}{[\epsilon - (\varepsilon_x - \omega_0)]^2 + [\Gamma_{1x,1x}/2]^2} + \text{Im} [G_{1x,1x}^<(\epsilon)] \frac{\epsilon - (\varepsilon_g + \omega_0)}{[\epsilon - (\varepsilon_g + \omega_0)]^2 + [\Gamma_{1g,1g}/2]^2} \right)$$

where $\mathbf{G}^<$ is the lesser projection of the Green function (7). Taking into account that in the absence of the chirp $E_{\text{inc}}(t) = \mathcal{E}_0 \cos(\omega_0 t)$ the first term in the right side of Eq.(19) suggests that for populated ground state, $G_{1g,1g}^<(\epsilon) \approx 1$, the molecular polarization oscillates in phase with the field for $\omega_0 < \varepsilon_x - \varepsilon_g$, and in anti-phase for $\omega_0 > \varepsilon_x - \varepsilon_g$. Thus according to Eqs. (15b) and (17) the molecular response quenches the field in the for-

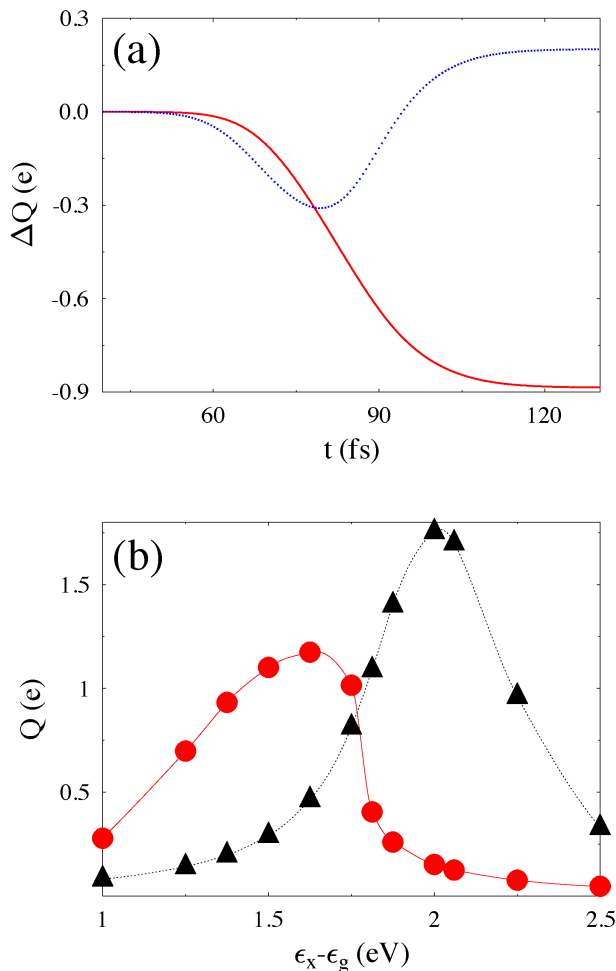


FIG. 4: (Color online) Charge pumped through the junction. (a) Difference, $\Delta Q \equiv Q^{(sc)} - Q^{(nosc)}$, between results calculated with, $Q^{(sc)}$, and without, $Q^{(nosc)}$, molecular response vs. time for $\varepsilon_x - \varepsilon_g > \omega_0$ (solid line, red) and $\varepsilon_x - \varepsilon_g < \omega_0$ (dotted line, blue). (b) Total charge pumped during the pulse vs. molecular excitation energy calculated without (triangles, black) and with (circles, red) molecular response. See text for parameters.

mer case, and enhances it in the latter. Fig. 3b illustrates this finding within the exact calculation showing the maximum of the total field for different molecular excitation energies (circles) compared to the maximum of the EM field obtained without molecular response (triangles). Note that contribution of the second term in the right side of Eq.(19) is exactly the opposite that of the first term, however since the calculations presented in Fig. 3 are performed at zero bias, the molecular excited state is initially empty, $G_{1x,1x}^<(t=0) \approx 0$.

While the local EM field cannot be measured directly, it is related to junction characteristics (in particular, its transport properties) detectable in experiments. Fig. 4a demonstrates the difference in the temporal buildup of the charge pumped through the junction, when the molecule is considered to be driven by the field obtained

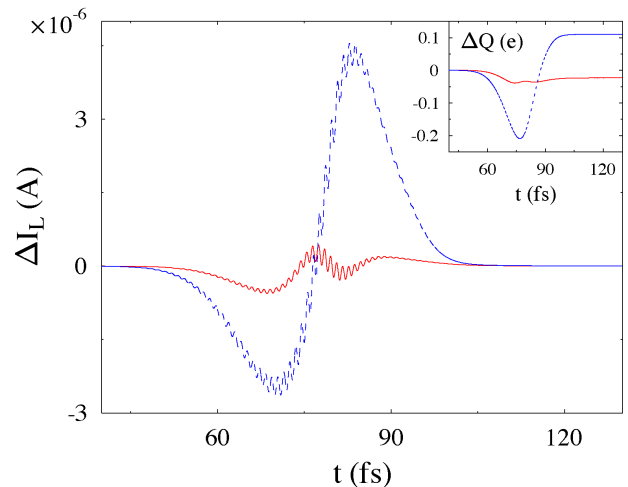


FIG. 5: (Color online) Current at the left interface as a function of time. Shown are differences, $\Delta I_L \equiv I_L^{(sc)} - I_L^{(nosc)}$, between results calculated with $I_L^{(sc)}$, and without, $I_L^{(nosc)}$, molecular response. The calculations are performed for $V_{sd} = 1.5$ V (dashed line, blue) and 2 V (solid line, red). Inset shows corresponding difference in charge pumped through the junction. See text for parameters.

within the self-consistent model vs. model with only SPP excitations taken into account. Initial dip in the charge buildup (see dotted line) is related to a time delay of the molecule induced pulse for $\varepsilon_x - \varepsilon_g < \omega_0$ (compare solid and dashed lines to the dotted line in Fig. 3a). The delay is caused by the chirped nature of the incoming pulse, with initial pulse frequency being lower than the molecular excitation energy, which results in suppression of the local field at the start of the pulse. Eventually however the incoming frequency becomes higher than the molecular transition energy. Corresponding enhancement of the local field leads to increase in the charge pumped through the junction. Note that for $\varepsilon_x - \varepsilon_g > \omega_0$ no delay is observed, and the local field is quenched throughout the pulse. Correspondingly effectiveness of the charge pump is lower in this case (see solid line in Fig. 4a).

Figure 4b shows the total charge pumped through the junction during the pulse at different molecular excitation energies. Clearly, the most effective EM field obtained without the molecular response taken into account corresponds to the resonance situation, $\omega_0 = \varepsilon_x - \varepsilon_g = 2$ eV. When molecular response is included in the model the situation is less straightforward. Since local field enhancement is expected for low molecular excitation energies, $\omega_0 > \varepsilon_x - \varepsilon_g$ (see Fig. 3b), the peak in the pumped charge distribution is shifted to the left. Note that the lower height of the shifted peak is related to the fact that, for a lower molecular gap, part of optical scattering channels is blocked due to partial population of the broadened excited and ground states of the molecule (see Ref. 49 for detailed discussion).

Note that the importance of molecular response de-

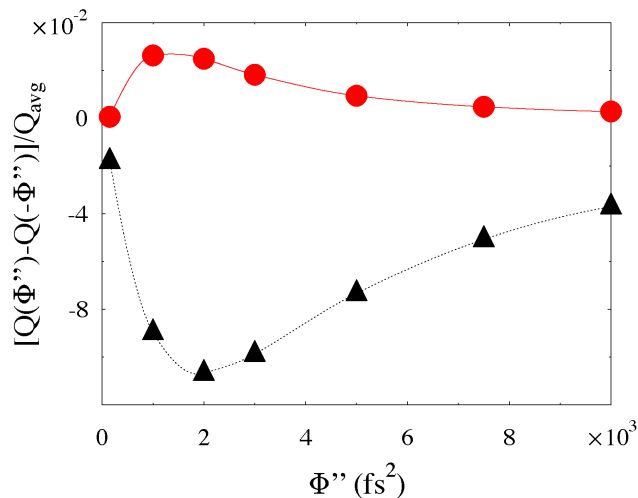


FIG. 6: (Color online) Asymmetry in the charge transfer between positively and negatively chirped incoming laser pulses, $Q(\Phi'') - Q(-\Phi'')$, normalized by their average, $Q_{avg} \equiv (Q(\Phi'') + Q(-\Phi''))/2$. Shown are results calculated without (triangles, black) and with (circles, red) the molecular response. See text for parameters.

depends also on bias across the junction. Indeed, since high bias, $V_{sd} > \varepsilon_x - \varepsilon_g$, may inject holes into the molecular ground state and electrons into the excited state, and since populating these states has opposite consequences for the local field enhancement (see Eq. (19) and the discussion following it), it is natural to expect that the molecular response is more important at low biases, $V_{sd} < \varepsilon_x - \varepsilon_g$. Figure 5 illustrates this conclusion with results of our calculations within the self-consistent model. Here $\Gamma_{1x,1x}^L = \Gamma_{1g,1g}^R = 0.05$ eV. We observe that both difference in optically induced current and charge pumped through the junction (see inset) is almost negligible at high biases. Similar reasoning indicates that the molecular response at strong incoming fields will be less important also due to population of the excited molecular state induced by external pulse.

Asymmetry in the charge pumping relative to the sign of the chirp rate was discussed in our recent publication (see Fig. 4 in Ref. 48). One of the reasons for the asymmetry is related to the time spent by the local pulse in the region of frequencies at and just below the resonance. This region provides the main contribution to charge transfer (see discussion of Fig. 3 in ref. 48). Since time spent in this region by the positively chirped pulse is smaller than that by the pulse with equal negative chirp rate (the positively chirped local pulse is shorter), one expects to observe an asymmetry as represented by the result of calculations using local EM field influenced only by SPP modes driving the junction (see curve with triangles in Fig. 6). However as discussed above, it is this pre-resonance region where molecular response quenches local field, thus diminishing (or even overturning) the asymmetry relative to the chirp rate sign (see curve with

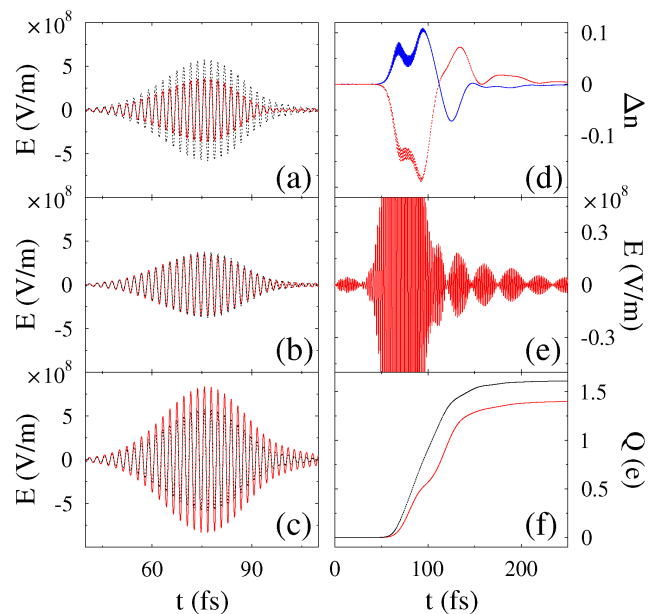


FIG. 7: (Color online) Effect of the self-consistent treatment on local field and level population in a 3-sites molecular bridge ($D = 3$) as functions of time. Shown are (a)-(c) local field calculated without (dotted line, black) and with ($\varepsilon_x - \varepsilon_g > \omega_0$ - solid line, red) molecular response for the three molecular sites. Panel (d) shows the difference in population of the ground, $\Delta n_{1g} \equiv n_{1g}^{(sc)} - n_{1g}^{(nosc)}$ (solid line, blue) and excited, $\Delta n_{1x} \equiv n_{1x}^{(sc)} - n_{1x}^{(nosc)}$ (dotted line, red) states for the first molecular site ($m = 1$). Panel (e) shows the scaled plot of the field on the central site ($m = 2$) for a longer period of time. The charge pumped through the 3-sites molecular bridge vs. time is shown in panel (f). See text for parameters.

circles in Fig. 6).

Finally, we consider a 3-sites molecular bridge ($D = 3$) to model the spacial nonlocality of molecular polarization. Calculations are done for $\varepsilon_{mx} - \varepsilon_{mg} = 2.25$ eV, $\omega_0 = 2$ eV, and $V_{sd} = 0$. Panels (a)-(c) of Fig. 7 compare the pure plasmonic local field to the field calculated when the molecular response is taken into account for the three sites of the bridge. Molecular polarization decreases the local field amplitude on the first site, (a), and enhances it on the rightmost site, (c). The field at the middle site, (b), does not change. The effect can be understood following the discussion similar to that of Fig. 3. We find that for $\varepsilon_x - \varepsilon_g > \omega_0$ increase in population in the ground (decrease in the excited) levels of the molecular sites quenches the local field. Change in the populations of the leftmost site, panel (a), resulting from self-consistent treatment is shown in Fig. 7d. We see that these changes are in agreement with the corresponding change in the local field. Similar considerations are also hold for panels (b) and (c) (corresponding level population are not shown).

Self-consistently calculated electric field on a site in the bridge shows a visible beat at large timescale (see Fig. 7e). This behavior is related to the Rabi frequency due to the

intersite coupling, t_s .

Finally, Fig 7f shows charge transferred through the 3-site junction as function of time. Decrease in the effectiveness of the pump is related to quenching of the local field on the first site of the bridge, where strong coupling to the left contact yields quick resupply of the ground level population. Decreased efficiency in pumping the charge between ground and excited levels at this site is the reason for the overall change in the effectiveness of the pump.

V. CONCLUSION

We consider a simple model of a molecular junction driven by external chirped laser pulses. The molecule is represented by a bridge of D two-level systems. The contacts geometry are taken in the form of a bowtie antenna. The FDTD technique is used to calculate the local field in the junction resulting from SPP excitations in the contacts. Simultaneously we solve time-dependent nonequilibrium Green functions equations of motion to take into account the molecular contribution to the local field formation.

Note that many works on driven transport assume pure incident field to be a driving force acting on the molecule. In our recent publications^{48,49} we considered effects of local field formation due to SPP excitations in the contacts on junction characteristics under external optical pumping. Here we make one more step by taking into account also the molecular response in the driving local field dynamics. Within a reasonable range of parameters we demonstrate that the latter is crucial for proper description of the junction transport. We compare our results with previously published predictions, and show that the molecular contribution may lead to measurable differences (both quantitative and qualitative) in characteristics of junctions. This contribution is especially important at low biases and relatively weak external fields in the presence of a strong molecular transition dipole. In particular, we show that for laser frequencies shorter (higher) than the molecular excitation energy the local SPP field is usually quenched (enhanced) by molecular response.

Extension of the approach to realistic *ab initio* calculations, taking into account time-dependent bias, and formulating a methodology for calculations in the language of molecular states are the goals for future research.

Acknowledgments

M.G. gratefully acknowledges support by the NSF (Grant No. CHE-1057930) and the BSF (Grant No. 2008282).

Appendix A: Derivation of Eq.(19)

To understand trends observed in the exact calculations based on Eqs. (9)-(10) and (15a)-(15b), here we employ a simple consideration and derive an approximate expression for the molecular polarization, Eq.(17), given in Eq.(19). For simplicity we assume that only one projection of the molecular dipole is non-zero, and consider a single molecule bridge ($D = 1$). Then the molecular polarization is

$$P_1(t) = -2\text{Im} [\mu_{xg} G_{1g,1x}^<(t, t)] \quad (\text{A1})$$

Assuming the dissipation matrix, Eq.(6), is diagonal the lesser projection of the Green function in Eq.(A1) is given by the Keldysh equation of the form

$$G_{1g,1x}^<(t, t) = \sum_{s=g,x} \int_{-\infty}^t dt_1 \int_{-\infty}^t dt_2 G_{1g,1s}^r(t, t_1) \times \Sigma_{1s,1s}^<(t_1 - t_2) G_{1g,1s}^r(t_2, t) \quad (\text{A2})$$

where

$$\Sigma_{1s,1s}^<(t_1 - t_2) = i \sum_{K=L,R} \int \frac{d\epsilon}{2\pi} f_K(\epsilon) \Gamma_{1s,1s}^K e^{-i\epsilon(t_1 - t_2)} \quad (\text{A3})$$

is the lesser self-energy due to coupling to the contacts.

We start by neglecting a chirp of the incoming field

$$E_{inc}(t) = \mathcal{E}_0 \cos(\omega_0 t) \quad (\text{A4})$$

and treat interaction between molecule and incoming field

$$V_{ss'}(t) \equiv -\delta_{s',\bar{s}} \mu_{s\bar{s}} E_{inc}(t) \quad (\text{A5})$$

within the first order of perturbation theory. Here \bar{s} indicates state opposite to s , i.e. for $s = g$ $\bar{s} = x$.

Within the approximations the retarded Green function in Eq.(A2) can be expressed as (similar expression can be written for the advanced projection)

$$G_{1s,1s'}^r(t, t') \approx \delta_{s,s'} G_{1s,1s}^{(0)r}(t - t') + \sum_{m,n=g,x} \int_{-\infty}^{+\infty} dt'' G_{1s,1s}^{(0)r}(t - t'') V_{ss'}(t'') G_{1s',1s'}^{(0)r}(t'' - t') \quad (\text{A6})$$

Here $\mathbf{G}^{(0)r}$ is the retarded projection of the Green functions (7) in the absence of external field

$$G_{1s,1s}^{(0)r}(t - t') = -i\theta(t - t') e^{-i(\epsilon_s - i\Gamma_{1s,1s}/2)(t - t')} \quad (\text{A7})$$

and $\theta(\dots)$ is the Heaviside step function.

Utilizing (A4)-(A7) in (A1)-(A3) leads to

$$P_1(t) \approx -\mathcal{E}_0 |\mu_{gx}|^2 \int \frac{d\epsilon}{2\pi} \left(\text{Im} \left[G_{1g,1g}^{(0)<}(\epsilon) \right] \frac{[\epsilon - (\epsilon_x - \omega_0)] \cos(\omega_0 t) - [\Gamma_{1x,1x}/2] \sin(\omega_0 t)}{[\epsilon - (\epsilon_x - \omega_0)]^2 + [\Gamma_{1x,1x}/2]^2} \right. \\ \left. + \text{Im} \left[G_{1x,1x}^{(0)<}(\epsilon) \right] \frac{[\epsilon - (\epsilon_g + \omega_0)] \cos(\omega_0 t) + [\Gamma_{1g,1g}/2] \sin(\omega_0 t)}{[\epsilon - (\epsilon_g + \omega_0)]^2 + [\Gamma_{1g,1g}/2]^2} \right) \quad (\text{A8})$$

where we have used the Keldysh equation for the steady state situation

$$G_{1s,1s}^{(0)<}(\epsilon) = \frac{\sum_{K=L,R} i f_K(\epsilon) \Gamma_{1s,1s}^K}{[\epsilon - \epsilon_s]^2 + [\Gamma_{1s,1s}/2]^2} \quad (\text{A9})$$

Assuming that detuning is much bigger than levels broad-

enings, $|\omega_0 - (\epsilon_x - \epsilon_g)| \gg \Gamma_{1s,1s}$ ($s = g, x$), the term with $\sin(\omega_0 t)$ in (A8) can be ignored. Finally, dressing the Green functions in Eq. (A8), i.e. taking into account diagrams related to population redistribution in the molecule due to presence of the driving field, leads to Eq.(19).

-
- * Electronic address: ajw009@ucsd.edu
 † Electronic address: maxim.sukharev@asu.edu
 ‡ Electronic address: migalperin@ucsd.edu
- ¹ E. Hutter and J. H. Fendler, J. H., *Adv. Materials* **16**, 1685-1706, (2004).
 - ² S. A. Maier and H. A. Atwater, H. A., *J. Appl. Phys.* **98**, 011101 (2005).
 - ³ A. V. Zayats, I. I. Smolyaninov, and A. A. Maradudin, *Phys. Rep.* **408**, 131-314 (2005).
 - ⁴ W. L. Barnes and W. A. Murray, *Adv. Materials* **19**, 3771-3782 (2007).
 - ⁵ N. J. Halas, *Nano Lett.* **10**, 3816-3822 (2010).
 - ⁶ M.I.Stockman, *Opt. Express*, **19**, 22029-22106 (2011).
 - ⁷ M. Pelton, J. Aizpurua, and G. Bryant, *Laser and Photonics Reviews* **2**, 136-159 (2008).
 - ⁸ M. A. Noginov, G. Zhu, A. M. Belgrave, R. Bakker, V. M. Shalaev, E. E. Narimanov, S. Stout, E. Herz, T. Suteewong, and U. Wiesner, *Nature* **460**, 1110-1112 (2009).
 - ⁹ N. Liu, L. Langguth, T. Weiss, J. Kastel, M. Fleischhauer, T. Pfau, and H. Giessen, *Nature Mater.* **8**, 758-762 (2009).
 - ¹⁰ A. K. Sarychev and V. M. Shalaev, *Electrodynamics of metamaterials* (World Scientific, Singapore, 2007).
 - ¹¹ R. Quidant and V. P. Drachev, *Opt. Mater. Express* **1**, 1139-1140 (2011).
 - ¹² O. Hess, J. B. Pendry, S. A. Maier, R. F. Oulton, J. M. Hamm, and K. L. Tsakmakidis, *Nature Mater.* **11**, 573-584 (2012).
 - ¹³ M. I. Stockman, *New J. Phys.* **10**, 025031 (2008).
 - ¹⁴ A. Yurtsever and A. H. Zewail, *Nano Lett.* **12**, 3334-3338 (2012).
 - ¹⁵ K. R. Catchpole, K. R. and A. Polman, A., *Opt. Express* **16**, 21793-21800 (2008).
 - ¹⁶ A. Pors, A. V. Uskov, M. Willatzen, and I. E. Protsenko, *Opt. Commun.* **284**, 2226-2229 (2011).
 - ¹⁷ E. D. Mammo, J. Marques-Hueso, and B. S. Richards, *Proceedings of the SPIE* **8438**, 84381M (2012).
 - ¹⁸ M. G. Reuter, M. Sukharev, and T. Seideman, *Phys. Rev. Lett.* **101**, 208303 (2008).
 - ¹⁹ V. Giannini, A. I. Fernandez-Dominguez, Y. Sonnefraud, T. Roschuk, R. Fernandez-Garcia, S. A. Maier, *Small* **6**, 2498-2507 (2010).
 - ²⁰ M. Artamonov and T. Seideman, *Nano Lett.* **10**, 4908-4912 (2010).
 - ²¹ J. Homola, *Anal. Bioanal. Chem.* **377**, 528-539 (2003).
 - ²² M. Delcea, N. Sternberg, A. M. Yashchenok, R. Georgieva, H. Baumler, H. Mohwald, and A. G. Skirtach, *ACS Nano* **6**, 4169-4180 (2012).
 - ²³ T. Sannomiya and J. Voros, *Trends in Biotechnology* **29**, 343-351 (2011).
 - ²⁴ F. Eftekhari, C. Escobedo, J. Ferreira, X. B. Duan, E. M. Girotto, A. G. Brolo, R. Gordon, and D. Sinton, *Anal. Chem.* **81**, 4308-4311 (2009).
 - ²⁵ S. K. Gray and T. Kupka, *Phys. Rev. B* **68**, 045415 (2003).
 - ²⁶ J. Yelk, M. Sukharev, and T. Seideman, *J. Chem. Phys.* **129**, 064706 (2008).
 - ²⁷ A. Coomar, C. Arntsen, K. A. Lopata, S. Pistinner, and D. Neuhauser, *J. Chem. Phys.* **135**, 084121 (2011).
 - ²⁸ A.-I. Henry, J. M. Bingham, E. Ringe, L. D. Marks, G. C. Schatz, and R. P. Van Duyne, *J. Phys. Chem. C* **115**, 9291-9305 (2011).
 - ²⁹ J. M. McMahon, S. Li, L. K. Ausman, and G. C. Schatz, *J. Phys. Chem. C* **116**, 1627-1637 (2012).
 - ³⁰ J. Zuloaga, E. Prodan, and P. Nordlander, *Nano Lett.* **9**, 887-891 (2009).
 - ³¹ S. M. Morton, D. W. Silverstein, and L. Jensen, *Chem. Rev.* **111**, 3962-3994 (2011).
 - ³² M. Sukharev and A. Nitzan, *Phys. Rev. A* **84**, 043802 (2011).
 - ³³ D. L. Jeanmaire and R. P. Van Duyne, *J. Electroanal. Chem.* **84**, 1-20 (1977).
 - ³⁴ S. Nie and S. R. Emory, *Science* **275**, 1102-1106 (1997).
 - ³⁵ J. Zhang, Y. Fu, M. H. Chowdhury, and J. R. Lakowicz, *Nano Lett.* **7**, 2101-2107 (2007).
 - ³⁶ Z. Ioffe, T. Shamai, A. Ophir, G. Noy, I. Yutsis, K. Kfir, O. Cheshnovsky, and Y. Selzer, *Nature Nanotech.* **3**, 727-732 (2008).
 - ³⁷ D. R. Ward, N. J. Halas, J. W. Ciszek, J. M. Tour, Y. Wu, P. Nordlander, and D. Natelson, *Nano Lett.* **8**, 919-924 (2008).
 - ³⁸ S. W. Wu, G. V. Nazin, and W. Ho, *Phys. Rev. B* **77**, 205430 (2008).
 - ³⁹ H. P. Yoon, M. M. Maitani, O. M. Cabarcos, L. Cai, T. S. Mayer, and D. L. Allara, *Nano Lett.* **10**, 2897-2902 (2010).
 - ⁴⁰ D. R. Ward, D. A. Corley, J. M. Tour, and D. Natelson,

- Nature Nanotech. **6**, 33-38 (2011).
- ⁴¹ K. Lopata and D. Neuhauser, J. Chem. Phys. **130**, 104707 (2009).
- ⁴² K. Lopata and D. Neuhauser, J. Chem. Phys. **131**, 014701 (2009).
- ⁴³ C. Arntsen, K. Lopata, M. R. Wall, L. Bartell, and D. Neuhauser, J. Chem. Phys. **134**, 084101 (2011).
- ⁴⁴ A. Salomon, R. J. Gordon, Y. Prior, T. Seideman, and M. Sukharev, Phys. Rev. Lett. **109**, 073002 (2012).
- ⁴⁵ Y. Gao and D. Neuhauser, J. Chem. Phys. **137**, 074113 (2012).
- ⁴⁶ J. Mullin and G. C. Schatz, J. Phys. Chem. A **116**, 1931-1938 (2012).
- ⁴⁷ M. Galperin and A. Nitzan, Phys. Chem. Chem. Phys. **14**, 9421-9438 (2012).
- ⁴⁸ B. D. Fainberg, M. Sukharev, T.-H. Park, and M. Galperin, Phys. Rev. B **83**, 205425 (2011).
- ⁴⁹ M. Sukharev and M. Galperin, Phys. Rev. B **81**, 165307 (2010).
- ⁵⁰ B. Lukýanchuk, N. I. Zheludev, S. A. Maier, N. J. Halas, P. Nordlander, H. Giessen, and C. T. Chong, Nature Mater. **9**, 707-715 (2010).
- ⁵¹ G. Li, M. S. Shishodia, B. D. Fainberg, B. Apter, M. Oren, A. Nitzan, and M. A. Ratner, Nano Lett. **12**, 2228-2232 (2012).
- ⁵² U. Peskin and M. Galperin, J. Chem. Phys. **136**, 044107 (2012).
- ⁵³ T.-H. Park and M. Galperin, Europhys. Lett. **95**, 27001 (2011).
- ⁵⁴ T.-H. Park and M. Galperin, Phys. Rev. B **84**, 075447 (2011).
- ⁵⁵ L. X. Wang and V. May, J. Phys. Chem. C **114**, 41794185 (2010).
- ⁵⁶ G. Q. Li, B. D. Fainberg, A. Nitzan, S. Kohler, and P. Hanggi, Phys. Rev. B **81**, 165310 (2010).
- ⁵⁷ M. Galperin, M. A. Ratner, and A. Nitzan, J. Chem. Phys. **130**, 144109 (2009).
- ⁵⁸ J. K. Viljas, F. Pauly, and J. C. Cuevas, Phys. Rev. B **77**, 155119 (2008).
- ⁵⁹ B. D. Fainberg, M. Jouravlev, and A. Nitzan, Phys. Rev. B **76**, 245329 (2007).
- ⁶⁰ J. K. Viljas, F. Pauly, and J. C. Cuevas, Phys. Rev. B **76**, 033403 (2007).
- ⁶¹ M. Galperin and A. Nitzan, J. Chem. Phys. **124**, 234709 (2006).
- ⁶² S. Kohler, J. Lehmann, and P. Hanggi, Phys. Rep. **406**, 379-443 (2005).
- ⁶³ A.-P. Jauho, N. S. Wingreen, and Y. Meir, Phys. Rev. B **50**, 5528-5544 (1994).
- ⁶⁴ H. Haug and A.-P. Jauho, *Quantum Kinetics in Transport and Optics of Semiconductors* (Springer-Verlag, Berlin, 2008).
- ⁶⁵ G. D. Mahan, *Many-Particle Physics* (Plenum Press, New York, 1990).
- ⁶⁶ M. Galperin and S. Tretiak, J. Chem. Phys. **128**, 124705 (2008).
- ⁶⁷ A. Taflove and S. C. Hagness, Susan C., *Computational electrodynamics: the finite-difference time-domain method* (Artech House, 2005).
- ⁶⁸ <http://plasmon.poly.asu.edu>
- ⁶⁹ A. Manjavacas, F. J. G. d. Abajo, and P. Nordlander, Nano Lett. **11**, 2318-2323 (2011).
- ⁷⁰ A. J. White, B. Fainberg, and M. Galperin (to be published).
- ⁷¹ J. M. Mullin, J. Autschbach, and G. C. Schatz, Comp.Theor. Chem. **987**, 32-41 (2012).